Published in final edited form as:
Oncogene. 2012 January 19; 31(3): 269–281. doi:10.1038/onc.2011.245.

Small molecule inhibitors of ezrin inhibit the invasive phenotype of osteosarcoma cells

G Bulut[1], **S-H Hong**[2], **K Chen**[1], **EM Beauchamp**[1], **S Rahim**[1], **GW Kosturko**[1], **E Glasgow**[1], **S Dakshanamurthy**[1], **H-S Lee**[3], **I Daar**[3], **JA Toretsky**[1], **C Khanna**[2], and **A Üren**[1]

[1]Georgetown University Medical Center, Lombardi Comprehensive Cancer Center, Washington, DC, USA

[2]Tumor and Metastasis Biology Section, Center for Cancer Research, National Cancer Institute, Bethesda, MD, USA

[3]Laboratory of Cell and Developmental Signaling, National Cancer Institute-Frederick, Frederick, MD, USA

Abstract

Ezrin is a multifunctional protein that connects the actin cytoskeleton to the extracellular matrix through transmembrane proteins. High ezrin expression is associated with lung metastasis and poor survival in cancer. We screened small molecule libraries for compounds that directly interact with ezrin protein using surface plasmon resonance to identify lead compounds. The secondary functional assays used for lead compound selection included ezrin phosphorylation as measured by immunoprecipitation and *in vitro* kinase assays, actin binding, chemotaxis, invasion into an endothelial cell monolayer, zebrafish and *Xenopus* embryonic development, mouse lung organ culture and an *in vivo* lung metastasis model. Two molecules, NSC305787 and NSC668394, that directly bind to ezrin with low micromolar affinity were selected based on inhibition of ezrin function in multiple assays. They inhibited ezrin phosphorylation, ezrin–actin interaction and ezrin-mediated motility of osteosarcoma (OS) cells in culture. NSC305787 mimicked the ezrin morpholino phenotype, and NSC668394 caused a unique developmental defect consistent with reduced cell motility in zebrafish. Following tail vein injection of OS cells into mice, both molecules inhibited lung metastasis of ezrinsensitive cells, but not ezrin-resistant cells. The small molecule inhibitors NSC305787 and NSC668394 demonstrate a novel targeted therapy that directly inhibits ezrin protein as an approach to prevent tumor metastasis.

Keywords

ezrin; osteosarcoma; metastasis; small molecule screening; drug discovery

Introduction

Osteosarcoma (OS) is the most common primary bone cancer type in children and adolescents (Longhi *et al.*, 2006). Its underlying pathogenesis has been difficult to establish because of its heterogeneous histology and complex etiology. Historically, patients with

Correspondence: Dr A Üren, Georgetown University Medical Center, Lombardi Comprehensive Cancer Center, 3970 Reservoir Rd. NW, NRB, Room E312, Washington, DC 20057, USA. au26@georgetown.edu.

Conflict of interest The authors declare no conflict of interest.

Supplementary Information accompanies the paper on the Oncogene website (http://www.nature.com/onc)

only localized disease have been treated with surgery alone, resulting in a 20% survival rate due to undetected micrometastasis likely present at diagnosis. Treatment of localized disease has improved with neoadjuvant chemotherapy, which has increased the 5-year survival to 60–70%. However, the 5-year survival of patients with metastasis is still only 30% (Rosen *et al.*, 1982; Bacci *et al.*, 2006; Ferrari and Palmerini, 2007; Zhang *et al.*, 2008). In OS, the predominant recurrence site is the lung and the main cause of OS patient death is pulmonary metastasis (Dunn and Dehner, 1977). Targeting the underlying molecular events that cause metastasis could provide dramatic benefits for the treatment of OS patients.

Ezrin, an ***ezrin/radixin/moesin (ERM) family member, is evolutionarily conserved both structurally and functionally (Fievet *et al.*, 2007). By regulating membrane-cytoskeleton complexes, ezrin has key roles in normal cellular processes such as maintenance of membrane dynamics, survival, adhesion, motility, cytokinesis, phagocytosis and integration of membrane transport with signaling pathways (Bretscher *et al.*, 2002). Ezrin function is actively regulated by its conformational changes (Fievet *et al.*, 2007). Ezrin exists in an inactive conformation, in which the membrane and actin-binding sites are masked by intramolecular interaction of the N-terminal and C-terminal domains (Gary and Bretscher, 1995). In its active open conformation, ezrin functions as a crosslinker between the plasma membrane and cortical cytoskeleton. Two factors are involved in this conformational transition: binding of the N-terminal domain to phosphatidylinositol 4,5-biphosphate and phosphorylation of a conserved threonine at residue 567 (T567) in the F-actin-binding site (Fievet *et al.*, 2007). Several serine/threonine kinases, Rho kinase, protein kinase C-alpha (PKCα) and iota (PKCI), and MST4 are important for T567 phosphorylation (Matsui *et al.*, 1998; Ren *et al.*, 2009; Ten Klooster *et al.*, 2009). Ezrin exhibits no intrinsic enzymatic activity and exerts its biological functions through protein–protein interactions. In its active form, ezrin can interact with membrane proteins either directly or through adapter proteins. It binds directly to adhesion-related proteins with single transmembrane domains such as CD43, CD44, CD95, ICAM-1, -2, -3 and PA2.26 antigen through their cytoplasmic tails (Louvet-Vallee, 2000), and this binding modulates cell motility and morphology (Legg and Isacke, 1998). Ezrin binding to adapter proteins such as EBP50/NHE-RF and E3KARP regulates the activity of ion transporters, endocytosis of plasma membrane proteins and interaction of F-actin to specific plasma membrane domains (Bretscher *et al.*, 2002). In addition to plasma membrane proteins, ezrin associates with cytoplasmic signaling proteins and is involved in several signaling pathways, such as Rho and PI3K/Akt pathways (Hirao *et al.*, 1996; Gautreau *et al.*, 1999).

In an OS mouse model, high ezrin expression is linked to pulmonary metastasis, providing an early survival advantage for cancer cells reaching the lung (Khanna *et al.*, 2004). Higher expression of ezrin correlates with poor prognosis in both canine and human OS. Comparison of ezrin expression in high- and low-grade human OS tumor samples revealed a clear correlation between ezrin expression and survival (Park *et al.*, 2006). In addition to OS, ezrin has been associated with tumor progression, metastatic spread and poor clinical outcome in several other cancers, including breast, colon, malignant melanoma, ovarian carcinoma, brain tumors and soft tissue sarcomas (Geiger *et al.*, 2000; Makitie *et al.*, 2001; Elliott *et al.*, 2005; Weng *et al.*, 2005; Kobel *et al.*, 2006; Elzagheid *et al.*, 2008). Consequently, suppression of ezrin expression in experimental models results in reduced metastasis (Makitie *et al.*, 2001; Khanna *et al.*, 2004; Pang *et al.*, 2004; Yu *et al.*, 2004).

In summary, accumulating evidence from experimental mouse models, as well as canine and human patients, validates ezrin as a key factor in cancer cell invasion and survival at metastatic sites. In the present study, we identified two small molecules, NSC305787 and NSC668394, which directly interact with ezrin and inhibit its function in multiple assays.

Results

Initial screening of small molecules for direct binding to ezrin

We hypothesized that small molecules that directly bind ezrin may inhibit its function and can potentially be developed as anti-metastatic agents for human malignancies. We screened small molecule libraries to identify compounds that directly bind to ezrin by expressing wild-type (WT) recombinant ezrin in bacteria and purifying it by column chromatography (Reczek *et al.*, 1997). We prepared recombinant WT ezrin at 100 μg/ml (1.25 μM) with >90% purity (Figure 1a). To validate that bacteria-purified, recombinant mouse ezrin has the appropriate tertiary structure, we evaluated its actin-binding ability. Threonine phosphorylation at amino acid residue 567 provides an open conformation of ezrin and increases its actin-binding capacity. We used threonine (T) to aspartic acid (D) substitution to mimic phosphorylation at this residue (Gautreau *et al.*, 2000) and subsequently purified WT and phosphomimicking mutant (T567D) forms of ezrin (Figure 1a). Actin binding of these two constructs was evaluated by immunoprecipitation. Cell lysates from low-ezrin-expressing K12 OS cells were incubated with recombinant ezrin. Cellular actin co-immunoprecipitated with recombinant ezrin was detected by immunoblotting. Significantly higher levels of actin bound to T567D ezrin than to WT ezrin (Figure 1b). We also observed increased binding of T567D ezrin to purified actin in an enzyme-linked immunosorbent assay (Supplementary Figure 1). These results suggested that at least a portion of recombinant ezrin made in bacteria was folded properly to replicate the expected mammalian structure.

Surface plasmon resonance (SPR) allows the measurement of direct molecular interactions in real-time and in a label-free setting (Fivash *et al.*, 1998; Malmqvist, 1999). We used SPR to screen small molecule libraries for compounds that directly bind to recombinant WT ezrin. Ezrin was immobilized on Biacore T100 sensorchips (GE Healthcare, Piscataway, NJ, USA), and small molecules were individually injected over the surface at a single concentration. We screened 3081 small molecules from four libraries (Challenge Set, Diversity Set, Mechanistic Set and Natural Product Set) provided by the Developmental Therapeutics Program of the National Cancer Institute. In this initial screen, any molecule demonstrating meaningful binding to recombinant ezrin over background values was selected as a primary hit. We then evaluated 65 primary hits in functional assays, which identified two lead compounds, NSC305787 and NSC668394 (Figure 1c). Detailed SPR analyses of the two compounds in five independent experiments yielded an average K_D of 5.85 μM (±3.85 μM (standard deviation (s.d.))) for the affinity of NSC305787 (Figure 1d) and 12.59 μM (±6.35 μM) for the affinity of NSC668394 (Figure 1e) binding to ezrin. K_D values of NSC305787 and NSC668394 binding to actin (used as a negative control) were 91.4 μM and 603 μM, respectively (data not shown). None of the 65 primary hits showed differential binding between WT and T567D ezrin. We also performed molecular docking studies to analyze the likely binding model of NSC305787 and NSC668394 with ezrin (Supplementary Figures 2 and 3). Analyses of the simulated models suggest that the two compounds are buried well inside the binding pockets of site 1 (H48, W58, Y85, Q105, I115, Y201 and N204) and site 2 (W278, L274, F250, P272 and L281).

Secondary functional assays used for lead compound selection included ezrin phosphorylation, actin binding, chemotaxis, invasion into an endothelial cell monolayer, zebrafish and *Xenopus* embryonic development, mouse lung organ culture and an *in vivo* lung metastasis model.

Additionally, druggability based on solubility, potential *in vivo* toxicity, chemical stability and derivatization potential were considered for elimination of some primary hits. We used Lipinski's 'Rule of Five', which is a classic predictor of the potential 'druggability' of a

small molecule, based on its physico-chemical properties. These parameters include the number of hydrogen bond donor and accepting groups present in the compound, the molecular weight and the calculated partition coefficient. Both NSC305787 and NSC668394 possess a functionalized quinoline pharmacophore, a molecular framework prevalent in clinical therapeutics. Computational analysis of both compounds with Chemdraw, SciFinder and MolInspiration software programs revealed the predicted partition coefficient of 5.8 for NSC305787 and 2.8 for NSC668394. Moreover, the molecular weights of 443 g/mol (NSC305787) and 450 g/mol (NSC668394), as well as total number of hydrogen bond accepting and donating moieties (three for NSC305787 and seven for NSC668394) were all within delineated parameters of this methodology, demonstrating the therapeutic promise of these scaffolds. Results of functional assays for NSC305787 and NSC668394 are presented in the following sections.

NSC305787 and NSC668394 inhibit ezrin T567 phosphorylation and actin binding

Ezrin T567 phosphorylation is critical for its activation, enabling the interaction of ezrin with other cellular proteins such as actin (Matsui *et al.*, 1998). Dynamic regulation of ezrin phosphorylation during metastatic progression is linked to PKC activation. Members of this serine/threonine kinase family that phosphorylate ezrin at T567 in OS cells include PKCα, I and γ (Ren *et al.*, 2009). We examined effects of NSC305787 and NSC668394 on *in vitro* ezrin phosphorylation by PKCI. PKCI phosphorylation of recombinant ezrin was inhibited by NSC305787 with an IC_{50} of 8.3 μM (Figure 2a) and by NSC668394 with an IC_{50} of 8.1 μM (Figure 2b). To determine whether reduced ezrin phosphorylation resulted from kinase inhibition, we tested the effect of the lead compounds on three PKC isoforms (PKCI, α and γ) using a non-specific substrate (myelin basic protein). To inhibit all three PKC isoforms, NSC305787 required higher concentration than that required to inhibit ezrin phosphorylation (Figure 2a). NSC668394 did not show any significant inhibition of PKC activity at the doses tested in the present study (maximum, 100 μM) (Figure 2b). Additionally, direct interaction experiments with Biacore revealed significantly weaker binding affinity for PKCI compared with ezrin: NSC305787 and NSC668394 bound to PKCI with K_D values of 172.4 μM and 58.1 μM, respectively (data not shown). These results strongly suggest that NSC305787 and NSC668394 inhibit ezrin T567 phosphorylation primarily via their binding to ezrin and not through inhibition of PKCI kinase activity. We also analyzed the effect of both compounds on PKCI phosphorylation of other ERM family members, radixin and moesin by using similar *in vitro* kinase assays (Supplementary Figure 4). The IC_{50} value for NSC305787 on PKCI phosphorylation of moesin was 9.4 μM, whereas IC_{50} value for NSC305787 on PKCI phosphorylation of radixin was 55 μM. IC_{50} values for NSC668394 on PKCI phosphorylation of moesin and radixin were 59.5 and 35.3 μM, respectively. These data on *in vitro* kinase assays of ezrin, myelin basic protein (non-ezrin substrate) and other ERM family members are summarized in Supplementary Table 1.

In addition, we tested the effect of NSC305787 and NSC668394 on phosphorylation and actin binding of endogenous ezrin in highly metastatic K7M2 OS cells. Both NSC305787 and NSC668394 inhibited T567 phosphorylation and actin binding of endogenous ezrin at 10 μM without altering cellular ezrin levels (Figure 2c).

OS cell invasion is inhibited by NSC305787 and NSC668394

Higher levels of ezrin expression in K7M2 cells compared with K12 cells led to enhanced metastatic potential of K7M2 cells (Figure 3a) (Khanna *et al.*, 2001). We tested all 65 initial hits for inhibition of cell motility of both cell lines in a modified Boyden chamber (Neuro Probe, Inc., Gaithersburg, MD, USA) chemotaxis assay. Any molecule that inhibited chemotaxis without cellular toxicity was given higher priority. The anti-invasive potential of

NSC305787 and NSC668394 was further validated using an electric cell impedance sensing system involving real-time measurement of changes in cell resistance as a human umbilical vein endothelial cells (HUVEC) monolayer was disrupted by invading tumor cells. Both NSC305787 and NSC668394 inhibited invasion by K7M2 cells on the HUVEC monolayer (Figures 3b and c). This inhibition at 10 μM was statistically different from that of dimethyl sulfoxide (DMSO) (1%) control at 5 h ($P = 0.0137$ and $P = 0.0020$, respectively; *t*-test). NSC305787 and NSC668394 demonstrated no effect on invasion by K12 cells. Neither compound was cytotoxic to K7M2 cells, K12 cells or HUVECs at this concentration in cell viability assays (data not shown). Furthermore, we performed a cellular migration assay in K7M2 cells to analyze any potential synergy between both compounds using the electric cell impedance sensing system. The IC_{50} values obtained from this assay were very much similar suggesting that the compounds do not show any synergy (Supplementary Figure 5).

NSC305787 and NSC668394 inhibit cell motility during zebrafish and Xenopus embryonic development

In zebrafish studies with ezrin, direct changes in interaction patterns have not been reported. In mesendodermal cells, ezrin2 (the zebrafish homolog) was shown to be activated by phosphorylation on the C-terminal threonine residue and was required for proper germ layer morphogenesis during gastrulation (Link *et al.*, 2006). Inhibition of ezrin2 expression by morpholino anti-sense oligonucleotides (MO) results in an unique phenotype in zebrafish embryos (Link *et al.*, 2006). Therefore, we tested the effect of the 65 primary hit compounds on early zebrafish embryonicdevelopment. Small molecules that killed embryos before 70% epiboly during gastrulation were eliminated based on toxicity. The ezrin MO phenotype, characterized by reduced epiboly movements resulting from defective germ layer morphogenesis, was confirmed by microinjection of MO as described by Link *et al.* (Figures 4a and e). Treatment with 10-μM NSC305787 mimicked the ezrin MO phenotype (Figures 4b and e). Embryos treated with 10-μM NSC668394 showed normal development at earlier stages, but had a very distinctive cycloptic eye phenotype by 28 h after fertilization (hpf) (Figures 4c and e). When NSC668394 was removed before 48 hpf, the animals survived up to 7 days and were able to swim, and their cycloptic eyes were otherwise functional as the single eye moved and responded to light (Figures 4d and e). In normal zebrafish development, the eye field extends across the midline, and as progenitor cells divide, they move laterally to form two separate eyes. Therefore, the observed cycloptic phenotype suggests stalling of eye precursor cells in the midline.

We also tested the effect of NSC305787 and NSC668394 on *Xenopus* embryonic development. Following treatment with 10-μM NSC305787, the embryos exhibited gastrulation defects at stage 12.5, while NSC668394-treated embryos showed very mild effects. By stage 37, both compounds (10 μM) caused delays in development and ventral defects. By stage 50, embryos had short and bent tails and reduced eyes, suggesting inhibition of cell motility (Supplementary Figure 6). Treatment with high concentrations (40 μM) of compounds caused severe gastrulation defects and embryonic death. Because no validated ezrin MO exists in *Xenopus*, we could not confirm that the observed phenotype in *Xenopus* was ezrin-specific.

Prevention of metastatic growth in a lung organ culture assay

In OS, the predominant site of recurrence is the lung, and the main cause of OS patient death is pulmonary metastasis (Dunn and Dehner, 1977). Metastasis is a multi-step process, involving invasion, extravasation and survival at the distant site. To evaluate the inhibitory potential of the lead compounds on pulmonary metastatic growth, we performed an *ex vivo* mouse lung organ culture assay. This method measures the effect on survival at the metastatic site. In this method, tumor cells reaching the lung following tail vein injection

grow in the lung slices maintained in organ culture, resembling *in vivo* lung metastasis (Mendoza *et al.*, 2010). When green fluorescent protein (GFP)-expressing K7M2 cells were injected through tail veins, metastatic foci were scored in lung organ cultures, which then were quantitated by GFP intensity using fluorescence microscopy. Both NSC305787 ($P = 0.003$) and NSC668394 ($P = 0.0054$) significantly inhibited the lung metastases growth of high-ezrin-expressing K7M2 OS cells in this organ culture assay (Figures 5a and b).

NSC305787 and NSC668394 inhibit ezrin-dependent in vivo OS metastatic growth in mouse lung

After observing inhibition of lung metastatic growth in lung organ culture, we tested the effect of NSC305787 and NSC668394 in an *in vivo* lung metastasis model. Mice were injected with either GFP-expressing K7M2 or MNNG-HOS cells, and then treated with NSC305787 or NSC668394. Following injection of K7M2 cells through tail veins, vehicle-treated animals died because of progressive lung metastases within approximately 4 weeks (median survival = 28.5 days). NSC305787- and NSC668394-treated animals survived up to 50 and 49 days, respectively (Figure 6a). The overall survival of NSC305787-treated mice was significantly different from that of the vehicle-treated group ($P = 0.0337$). NSC668394-treated mice showed an increase in survival but this increase was not statistically significant from the vehicle group ($P = 0.0524$). When lung tissues were harvested and analyzed, we observed a significant decrease in the number of the GFP-expressing metastatic foci in the lung tissues of NSC305787- and NSC668394-treated groups (Figure 6b).

MNNG-HOS is an OS cell line with an ezrin-independent metastatic phenotype in contrast to K7M2 cells (Wan *et al.*, 2009). Thus, we used MNNG-HOS cells as a negative control for ezrin-dependent specificity. Animals injected with GFP-expressing MNNG-HOS cells by tail vein and treated with NSC305787 or NSC668394 demonstrated no difference in survival between control and treatment groups. The median survivals of vehicle-, NSC305787- and NSC668394-treated MNNG-HOS cells were 50.5, 49 and 48.5 days, respectively (Figure 6c). We observed no differences among the vehicle-, NSC305787- and NSC668394-treated groups regarding the number of GFP-expressing metastatic foci in lung tissues (Figure 6d).

Discussion

Ezrin is a key regulator in the progression and metastasis of pediatric tumors, including OS and rhabdomyosarcoma (Khanna *et al.*, 2004; Yu *et al.*, 2004). To develop ezrin-targeted therapy, we used SPR technology to screen 3081 small molecules that bind to ezrin and identified 65 initial hits. These small molecules were then evaluated biologically and biochemically for their potential to inhibit ezrin activity. NSC305787 and NSC668394 were selected based on their ability to inhibit ezrin function in multiple functional assays and their higher ezrin-binding affinity (~ 10 μM).

Our experiments were designed to discover small molecules that specifically inhibited ezrin function and were related to metastasis. Because ezrin loss does not affect cell viability in most cancer cells, we selectively discarded small molecules that were cytotoxic in either cell culture or zebrafish embryo assays. Therefore, we are the first to demonstrate that NSC305787 and NSC668394 directly target the anti-metastatic properties of ezrin. Our lead compounds inhibited ezrin T567 phosphorylation in the low micromolar range both *in vivo* and *in vitro*. During *in vivo* experiments, we did not observe a clear inhibition on the phosphoezrin levels in whole cell lysates, whereas in lysates immunoprecipitated with ezrin antibody, this inhibition on the phospho-ezrin protein levels was significant. This may be related to the specificity of the phosphoantibody, which recognized all three members of the ERM family. In *in vitro* experiments though, we were able to show stronger inhibition in phosphorylation levels of the T567 threonine residue on recombinant ezrin protein when

compared with the relevant threonine residues on other ERM members, radixin and moesin. Besides, we checked ezrin phosphorylation levels in our *in vivo* experiments. Phospho-ezrin levels were compared in lung–liver–kidney–spleen–skin samples between control (DMSO) vs NSC305787- and NSC668394- treated animals, but did not observe any meaningful differences. We believe that inhibition of ezrin phosphorylation is one of the mechanisms that NSC305787 and NSC668394 inhibit ezrin function. These lead compounds are likely to act through different mechanisms involving ezrin some of which may not require phosphorylated ezrin. Therefore, NSC305787 and NSC668394 inhibition of ezrin is still possible without inhibiting ezrin phosphorylation.

Targeted, direct small molecule binding to ezrin that reduces phosphorylation is a novel mechanism for the prevention of metastatic disease. We confirmed that both NSC305787 and NSC668394 inhibited the motility of metastatic murine OS cells with high ezrin expression. In a second confirmatory model, these compounds also inhibited mouse pulmonary metastases only in OS cells that require ezrin. This *in vivo* model not only supports that NSC305787 and NSC668394 eliminate ezrinmodulated metastases, but also the specificity of these compounds.

Although NSC305787 and NSC668394 possess potent anti-metastatic activities against OS cells through inhibition of ezrin function both *in vitro* and *in vivo*, the underlying molecular mechanisms remain poorly understood. Because ezrin lacks intrinsic enzymatic activity, it exhibits its biological functions through regulation of the cell cytoskeleton and activities of signaling pathways through protein–protein interactions. NSC305787 and NSC668394 may likely target protein interactions involving ezrin. T567 phosphorylation leads to a conformational change in the tertiary structure of ezrin by reducing the affinity of the C-terminal domain for the N-terminal 4.1/ERM (FERM) domain. This creates an open conformation allowing proteins such as F-actin to bind to ezrin (Gary and Bretscher, 1995). Two potential mechanisms of NSC305787- and NSC668394-mediated ezrin inhibition are reduced T567 phosphorylation and blocking protein–protein interactions directly involving ezrin. These two are not necessarily related to each other. It is possible to block protein–protein interactions of ezrin without affecting its phosphorylation levels. These *in vitro* experiments were performed by using WT and T567D forms of recombinant ezrin proteins that are synthesized in M15 bacteria, a derivative of *E.coli*. We have done several experiments to confirm that these proteins are properly folded based on better actin binding. However, these experiments can not establish what percentage of the total protein is in open form vs closed form. Furthermore, a computational structure analysis based on existing ezrin domain structures suggests several potential binding sites for NSC305787 and NSC668394 that are not on T567D. Binding of these small molecules may occur at multiple sites on ezrin leading to local conformational changes without directly interfering T567 phosphorylation site, but effecting interaction of other proteins with ezrin.

NSC305787 and NSC668394 both inhibited ezrin phosphorylation and showed mostly comparable effects on inhibiting ezrin functions *in vitro* and *in vivo*. However, clear divergence was found in different assays: NSC305787 treatment of zebrafish embryos mimicked the ezrin MO phenotype, whereas treatment with NSC668394 showed normal development at earlier stages, but demonstrated a distinctive cycloptic eye phenotype later in development (Figure 4). NSC305787 was more effective in preventing lung metastasis than NSC668394 (Figure 5). The compounds also revealed different binding kinetics: NSC305787 bound to and dissociated faster from ezrin than NSC668394. These results suggest that, although NSC305787 and NSC668394 both exhibit inhibitory effects on ezrin function, they likely exert these effects through different mechanisms such as altering different protein–protein interactions involving ezrin. Based on these results, we also tested any possible synergistic effect of NSC305787 and NSC668394 on K7M2 cellular migration,

but did not observe any combined inhibitory effect. It is important to note that high homology exists among ERM family proteins (Fehon *et al.*, 2010). Therefore, the observed results in this study could be partially due to inhibition of radixin and moesin as much as inhibition of ezrin. However, both NSC305787 and NSC668394 were very well tolerated *in vivo* without any obvious acute toxicity. When we performed maximum tolerable dose studies before our mouse experiments, all five animals in each group survived the 5-day intraperitoneal treatment of NSC305787 and NSC668394 at 2.4 and 2.26 mg/kg/day, respectively.

In conclusion, we targeted protein–protein interactions involving ezrin as a novel anti-metastatic therapy. Although future studies are required to evaluate the specificity of NSC305787 and NSC668394, their molecular frameworks possess a functionalized quinoline pharmacophore, which is a common motif in clinical therapeutics (Ohnmacht *et al.*, 1971; Boger *et al.*, 1987). Analysis of the molecular weight, hydrogen bonding moieties and predicted partition coefficient with Lipinski's rule-of-five analysis (Lipinski *et al.*, 2001) validated the drug-like composition of these compounds. Therefore, NSC305787 and NSC668394 can likely be developed as novel anti-ezrin compounds for clinical applications.

Materials and methods

Ezrin purification

Recombinant WT and T567D ezrin proteins were purified as described previously (Reczek *et al.*, 1997).

Immunoprecipitation and immunoblotting

Immunoprecipitation and immunoblotting were performed with ezrin (Sigma-Aldrich, St Louis, MO, USA), phosphoezrin (Cell Signaling, Danvers, MA, USA), and actin (Santa Cruz Biotechnology, Santa Cruz, CA, USA) antibodies as previously described (Ren *et al.*, 2009).

Enzyme-linked immunosorbent assay

Enzyme-linked immunosorbent assay experiments were performed by coating a 96-well plate with recombinant actin (Cytoskeleton, Inc., Denver, CO, USA) or bovine serum albumin. Non-specific binding sites were blocked with 200 μl of blocking reagent (Pierce, Rockford, IL, USA) for 2 h at room temperature. Wells were washed five times with phosphate-buffered saline-T (phosphate-buffered saline containing 0.05% Tween 20). Recombinant WT or T567D ezrin proteins were added and incubated for 2 h at room temperature. Following washes with phosphate-buffered saline-T, WT or T567D ezrin bound to actin protein was detected by an ezrin antibody and an horseradish peroxidase-conjugated anti-mouse antibody (Sigma-Aldrich). After a final washing step, 2,2′-azino-di-3-ethylbenzthiazline sulfonate (ABTS, Sigma-Aldrich) substrate was added and the optical density at 405 nm was read after 10 min.

SPR

Compounds were acquired from four libraries (Challenge Set, Diversity Set, Mechanistic Set and Natural Product Set) of the Developmental Therapeutics Program within National Cancer Institute. Their direct ezrin-binding potential was analyzed using the Biacore T100 instrument (GE Healthcare, Piscataway, NJ, USA). Recombinant WT ezrin protein was immobilized onto a Biacore CM5 sensorchip, and compounds were injected individually as the binding interactions were recorded. Any molecule giving more than 10 resonance units of binding signal with an acceptable curve shape was deemed an initial hit. Results were analyzed using the Biacore T-100 v2.0.3 analysis software (GE Healthcare).

Molecular modeling and docking studies

The X-ray crystal structure of Ezrin (PDB: 1NI2) was used for the molecular docking of NSC305787 and NSC668394. Ezrin structure was minimized with AMBER 9.0 (University of California, San Fransisco, CA, USA) (Case *et al.*, 2004) with SANDER default parameters. Docking experiments were performed using SurflexDock module of Sybyl 8.1 (Tripos International, St Louis, MO, USA) with a number of solution conformations were set to 90. The best docked geometry for compounds was energy minimized with SANDER module of AMBER9.0 (Case *et al.*, 2004).

Molecular dynamics simulations

To relax the docked complex, compounds docked models were subjected to molecular dynamics simulations using AMBER 9.0 (Case *et al.*, 2004) with the general amber force field (Wang *et al.*, 2004) and RMSD charge models (Bayly *et al.*, 1993). Molecular dynamics simulations performed in the micro canonical ensemble (NVE; moles (N), volume (V), energy (E) are conserved) consisted of an initial equilibration of 10 ps followed by a production run of 100 ps dynamics at 300 K. The final complex structure at the end of the molecular dynamics simulation was subjected to 2000 steps of steepest descent energy minimization followed by conjugate gradient energy minimization. A distance-dependent dielectric constant and non-bonded distance cutoff of 15Å were used.

In vitro kinase assay

Recombinant ezrin protein (500 ng) was incubated with the compounds at 1–100-μM concentrations for 15 min on ice, and then 50-ng PKCI (Millipore, Billerica, MA, USA) was added. Reactions were performed at 30 °C for 30 min and stopped by adding 2 × sample buffer. NSC305787 and NSC668394 profiling of PKCI, α and γ were performed on a non-specific substrate (myelin basic protein) using the Kinase Inhibitor Compound Profiling service (Kinexus Bioinformatics Corporation, Vancouver, BC, Canada).

Chemotaxis assay

Chemotaxis experiments were performed in 96-well Boyden chambers as described previously (Chen *et al.*, 2008). All 96-well chemotaxis assays were conducted in parallel with a 96-well viability assays to rule out toxicity. The WST viability assay was performed according to the manufacturer's protocol (Roche, Indianapolis, IN, USA).

Invasion assay

The anti-invasive potential of NSC305787 and NSC668394 was validated using the xCELLigence electric cell impedance system (Roche). Human umbilical vein endothelial cells (HUVECs; 2.5×10^4/well) were seeded in a 96-well plate in endothelial growth media-2 (Lonza, Basel, Switzerland). Following formation of a confluent HUVEC monolayer (~32 h), endothelial growth media-2 was aspirated and a layer of OS cells (1.0×10^4 cells/well) was added to Dulbecco's modified Eagle medium containing the compounds. This specific time point was accepted as 0 h of treatment, and invasion was monitored during the subsequent 5 h by measuring changes in resistance at the cell-electrode interphase. The cell index was calculated according to the following formula: cell index = $(R_t - R_0)/F$, where R_t is resistance at time point t, R_0 is background resistance (measured with media alone, no cells) and F is frequency at which the measurement was taken (10 kHz).

Cell migration assay

Cell migration experiments were performed using the CIM-plate 16 migration chamber from xCELLigence electric cell impedance system (Roche). A total volume of 150 μl containing

K7M2 cells (1.5×10^5 cells/well) and compounds at various concentrations were applied to the upper chamber in a serumfree media containing 1% DMSO. The lower chamber was loaded with 160 μl of a 10% fetal bovine serum media containing 1% DMSO as the chemoattractant. Cell migration was monitored in 'real-time' for a period of 24 h.

Zebrafish embryo development assay

Zebrafish were maintained as described previously (Westerfield, 1993). Embryo development was followed by morphological characterization (Kimmel *et al.*, 1995). For experiments involving MO injections, a translation-blocking anti-ezrin MO was synthesized by Gene-Tools, LCC (Philomath, OR, USA). This MO has been previously described and validated by Link *et al.* 2006. For chemical screening, zebrafish embryos were arrayed in 96-well plates. Compounds were added at 1–33-μM concentrations. Embryos were observed at 70% epiboly, 24–28 hpf and 48 hpf. All animal studies were approved by the Institutional Animal Care and Use Committee of Georgetown University.

Xenopus embryo development assay

Xenopus embryos were *in vitro* fertilized and cultured in 0.1X MBS (8.8 mM NaCl, 0.1 mM KCl, 0.1 mM MgSO4, 0.5 mM HEPES and 0.25 mM NaHCO3, (pH 7.8)) and treated with NSC305787 and NSC668394 blindly at the two-cell stage in 96-well plates.

Pulmonary metastasis assay

The technique of isolated lung organ culture was performed as reported by Mendoza *et al* (Mendoza *et al.*, 2010). Fresh media or compounds (10 μM) were replaced every other day. A LEICA-DM IRB fluorescence inverted microscope (Leica, Deerfield, IL) and Retiga-EXi Fast 1394 Mono Cooled CCD camera (Qimaging, Surrey, BC, Canada) were used to capture images of GFP-positive tumor cells within the pulmonary metastasis assay at × 100 magnification. Metastatic burden was quantified by measuring the fluorescent area of metastatic cells in each lung section at each time point and was expressed as mean fluorescent area (mean fluorescent area of each lung section over four lung sections). The mean fluorescent area was normalized to 100 pixels for day 0 to allow quantitative evaluation of metastatic progression over time.

In vivo experimental metastasis model

GFP-expressing K7M2 or MNNG-HOS tumor cells (1×10^6) were delivered by tail vein to female BALB/c (K7M2; Taconic, Hudson, NY, USA) or SCID/Beige (Charles Rivers, Wilmington, MA, USA) mice. One day after tumor cell injection, vehicle ($n = 10$) (dimethylsulfoxide (DMSO), 1%), NSC305787 ($n = 10$) (0.240 mg/kg/day) or NSC668394 ($n = 10$) (0.226 mg/kg/day) was administered 5-days a week by intraperitoneal injection. Mice were then monitored for evidence of morbidity including anorexia, dehydration, dyspnea and decreased activity and grooming behavior. Euthanasia of mice with presumed pulmonary metastases was based on the development of these symptoms. Animals were euthanized at day 66 regardless of these symptoms. All mice had necropsy to confirm metastatic lung disease. Animal studies were approved by an Institutional Animal Care and Use Committee of the National Institutes of Health.

Statistical analysis

Statistical analyses were performed using Prism version 4.0 (GraphPad Software, La Jolla, CA, USA). Statistical significance was defined as $P<0.05$.

Supplementary Material

Refer to Web version on PubMed Central for supplementary material.

Acknowledgments

Support for our work came from the Children's Cancer Foundation of Baltimore (AÜ), US Department of Defense (W81XWH-10-1-0137, AÜ), Brandon Carrington Lee Foundation (G.K., AÜ), Go4theGoal, Dani's Foundation, Alex's Lemonade Stand Foundation, Liddy Shriver Sarcoma Initiative, Burroughs Wellcome Clinical Scientist Award in Translational Research (JT), and the NIH R01CA133662 (JT), R01CA138212 (JT) and Cancer Center Support Grant P30 CA051008 for use of Biacore Molecular Interaction Shared Resource. We would like to thank to Dr Anthony Bretscher (Cornell University) for providing the WT Ezrin construct, Developmental Therapeutics Program, NCI for providing the small molecule libraries.

References

Bacci G, Longhi A, Cesari M, Versari M, Bertoni F. Influence of local recurrence on survival in patients with extremity osteosarcoma treated with neoadjuvant chemotherapy: the experience of a single institution with 44 patients. Cancer. 2006; 106:2701–2706. [PubMed: 16691623]

Bayly C, Cieplak P, Cornell WD, Kollman PA. A well-behaved electrostatic potential based method using charge restraints for deriving atomic charges: the RESP model. J Phys Chem. 1993; 97:10269–10280.

Boger DL, Yasuda M, Mitscher LA, Drake SD, Kitos PA, Thompson SC. Streptonigrin and lavendamycin partial structures. Probes for the minimum, potent pharmacophore of streptonigrin, lavendamycin, and synthetic quinoline-5,8-diones. J Med Chem. 1987; 30:1918–1928. [PubMed: 3656364]

Bretscher A, Edwards K, Fehon RG. ERM proteins and merlin: integrators at the cell cortex. Nat Rev Mol Cell Biol. 2002; 3:586–599. [PubMed: 12154370]

Case, DA.; Darden, TA.; Cheatham, TE., III; Simmerling, CL.; Wang, J.; Duke, RE., et al. AMBER 8. University of California at San Francisco; San Francisco: 2004.

Chen K, Fallen S, Abaan HO, Hayran M, Gonzalez C, Wodajo F, et al. Wnt10b induces chemotaxis of osteosarcoma and correlates with reduced survival. Pediatr Blood Cancer. 2008; 51:349–355. [PubMed: 18465804]

Dunn D, Dehner LP. Metastatic osteosarcoma to lung: a clinicopathologic study of surgical biopsies and resections. Cancer. 1977; 40:3054–3064. [PubMed: 271038]

Elliott BE, Meens JA, SenGupta SK, Louvard D, Arpin M. The membrane cytoskeletal crosslinker ezrin is required for metastasis of breast carcinoma cells. Breast Cancer Res. 2005; 7:R365–R373. [PubMed: 15987432]

Elzagheid A, Korkeila E, Bendardaf R, Buhmeida A, Heikkila S, Vaheri A, et al. Intense cytoplasmic ezrin immunoreactivity predicts poor survival in colorectal cancer. Hum Pathol. 2008; 39:1737–1743. [PubMed: 18701134]

Fehon RG, McClatchey AI, Bretscher A. Organizing the cell cortex: the role of ERM proteins. Nat Rev Mol Cell Biol. 2010; 11:276–287. [PubMed: 20308985]

Ferrari S, Palmerini E. Adjuvant and neoadjuvant combination chemotherapy for osteogenic sarcoma. Curr Opin Oncol. 2007; 19:341–346. [PubMed: 17545797]

Fievet B, Louvard D, Arpin M. ERM proteins in epithelial cell organization and functions. Biochim Biophys Acta. 2007; 1773:653–660. [PubMed: 16904765]

Fivash M, Towler EM, Fisher RJ. BIAcore for macromolecular interaction. Curr Opin Biotechnol. 1998; 9:97–101. [PubMed: 9503595]

Gary R, Bretscher A. Ezrin self-association involves binding of an N-terminal domain to a normally masked C-terminal domain that includes the F-actin binding site. Mol Biol Cell. 1995; 6:1061–1075. [PubMed: 7579708]

Gautreau A, Louvard D, Arpin M. Morphogenic effects of ezrin require a phosphorylation-induced transition from oligomers to monomers at the plasma membrane. J Cell Biol. 2000; 150:193–203. [PubMed: 10893267]

Gautreau A, Poullet P, Louvard D, Arpin M. Ezrin, a plasma membrane-microfilament linker, signals cell survival through the phosphatidylinositol 3-kinase/Akt pathway. Proc Natl Acad Sci USA. 1999; 96:7300–7305. [PubMed: 10377409]

Geiger KD, Stoldt P, Schlote W, Derouiche A. Ezrin immunoreactivity is associated with increasing malignancy of astrocytic tumors but is absent in oligodendrogliomas. Am J Pathol. 2000; 157:1785–1793. [PubMed: 11106550]

Hirao M, Sato N, Kondo T, Yonemura S, Monden M, Sasaki T, et al. Regulation mechanism of ERM (ezrin/radixin/moesin) protein/plasma membrane association: possible involvement of phosphatidylinositol turnover and Rho-dependent signaling pathway. J Cell Biol. 1996; 135:37–51. [PubMed: 8858161]

Khanna C, Khan J, Nguyen P, Prehn J, Caylor J, Yeung C, et al. Metastasis-associated differences in gene expression in a murine model of osteosarcoma. Cancer Res. 2001; 61:3750–3759. [PubMed: 11325848]

Khanna C, Wan X, Bose S, Cassaday R, Olomu O, Mendoza A, et al. The membrane-cytoskeleton linker ezrin is necessary for osteosarcoma metastasis. Nat Med. 2004; 10:182–186. [PubMed: 14704791]

Kimmel CB, Ballard WW, Kimmel SR, Ullmann B, Schilling TF. Stages of embryonic development of the zebrafish. Dev Dyn. 1995; 203:253–310. [PubMed: 8589427]

Kobel M, Gradhand E, Zeng K, Schmitt WD, Kriese K, Lantzsch T, et al. Ezrin promotes ovarian carcinoma cell invasion and its retained expression predicts poor prognosis in ovarian carcinoma. Int J Gynecol Pathol. 2006; 25:121–130. [PubMed: 16633060]

Legg JW, Isacke CM. Identification and functional analysis of the ezrin-binding site in the hyaluronan receptor, CD44. Curr Biol. 1998; 8:705–708. [PubMed: 9637922]

Link V, Carvalho L, Castanon I, Stockinger P, Shevchenko A, Heisenberg CP. Identification of regulators of germlayer morphogenesis using proteomics in zebrafish. J Cell Sci. 2006; 119:2073–2083. [PubMed: 16638810]

Lipinski CA, Lombardo F, Dominy BW, Feeney PJ. Experimental and computational approaches to estimate solubility and permeability in drug discovery and development settings. Adv Drug Deliv Rev. 2001; 46:3–26. [PubMed: 11259830]

Longhi A, Errani C, De Paolis M, Mercuri M, Bacci G. Primary bone osteosarcoma in the pediatric age: state of the art. Cancer Treat Rev. 2006; 32:423–436. [PubMed: 16860938]

Louvet-Vallee S. ERM proteins: from cellular architecture to cell signaling. Biol Cell. 2000; 92:305–316. [PubMed: 11071040]

Makitie T, Carpen O, Vaheri A, Kivela T. Ezrin as a prognostic indicator and its relationship to tumor characteristics in uveal malignant melanoma. Invest Ophthalmol Vis Sci. 2001; 42:2442–2449. [PubMed: 11581181]

Malmqvist M. BIACORE: an affinity biosensor system for characterization of biomolecular interactions. Biochem Soc Trans. 1999; 27:335–340. [PubMed: 10093759]

Matsui T, Maeda M, Doi Y, Yonemura S, Amano M, Kaibuchi K, et al. Rho-kinase phosphorylates COOH-terminal threonines of ezrin/radixin/moesin (ERM) proteins and regulates their head-to-tail association. J Cell Biol. 1998; 140:647–657. [PubMed: 9456324]

Mendoza A, Hong SH, Osborne T, Khan MA, Campbell K, Briggs J, et al. Modeling metastasis biology and therapy in real time in the mouse lung. J Clin Invest. 2010; 120:2979–2988. [PubMed: 20644255]

Ohnmacht CJ, Patel AR, Lutz RE. Antimalarials. 7. Bis(trifluoromethyl)- -(2-piperidyl)-4-quinolinemethanols. J Med Chem. 1971; 14:926–928. [PubMed: 5115690]

Pang ST, Fang X, Valdman A, Norstedt G, Pousette A, Egevad L, et al. Expression of ezrin in prostatic intraepithelial neoplasia. Urology. 2004; 63:609–612. [PubMed: 15028477]

Park HR, Jung WW, Bacchini P, Bertoni F, Kim YW, Park YK. Ezrin in osteosarcoma: comparison between conventional high-grade and central low-grade osteosarcoma. Pathol Res Pract. 2006; 202:509–515. [PubMed: 16677779]

Reczek D, Berryman M, Bretscher A. Identification of EBP50: A PDZ-containing phosphoprotein that associates with members of the ezrin-radixin-moesin family. J Cell Biol. 1997; 139:169–179. [PubMed: 9314537]

Ren L, Hong SH, Cassavaugh J, Osborne T, Chou AJ, Kim SY, et al. The actin-cytoskeleton linker protein ezrin is regulated during osteosarcoma metastasis by PKC. Oncogene. 2009; 28:792–802. [PubMed: 19060919]

Rosen G, Caparros B, Huvos AG, Kosloff C, Nirenberg A, Cacavio A, et al. Preoperative chemotherapy for osteogenic sarcoma: selection of postoperative adjuvant chemotherapy based on the response of the primary tumor to preoperative chemotherapy. Cancer. 1982; 49:1221–1230. [PubMed: 6174200]

Ten Klooster JP, Jansen M, Yuan J, Oorschot V, Begthel H, Di Giacomo V, et al. Mst4 and ezrin induce brush borders downstream of the Lkb1/Strad/Mo25 polarization complex. Dev Cell. 2009; 16:551–562. [PubMed: 19386264]

Wan X, Kim SY, Guenther LM, Mendoza A, Briggs J, Yeung C, et al. Beta4 integrin promotes osteosarcoma metastasis and interacts with ezrin. Oncogene. 2009; 28:3401–3411. [PubMed: 19597468]

Wang J, Wolf RM, Caldwell JW, Kollman PA, Case DA. Development and testing of a general amber force field. J Comput Chem. 2004; 25:1157–1174. [PubMed: 15116359]

Weng WH, Ahlen J, Astrom K, Lui WO, Larsson C. Prognostic impact of immunohistochemical expression of ezrin in highly malignant soft tissue sarcomas. Clin Cancer Res. 2005; 11:6198–6204. [PubMed: 16144921]

Westerfield, M. The Zebrafish book: a guide for the laboratory use of zebrafish (Brachydanio rerio). University of Oregon Press; Eugene Oregon: 1993.

Yu Y, Khan J, Khanna C, Helman L, Meltzer PS, Merlino G. Expression profiling identifies the cytoskeletal organizer ezrin and the developmental homeoprotein six-1 as key metastatic regulators. Nat Med. 2004; 10:175–181. [PubMed: 14704789]

Zhang P, Yang Y, Zweidler-McKay PA, Hughes DP. Critical role of notch signaling in osteosarcoma invasion and metastasis. Clin Cancer Res. 2008; 14:2962–2969. [PubMed: 18483362]

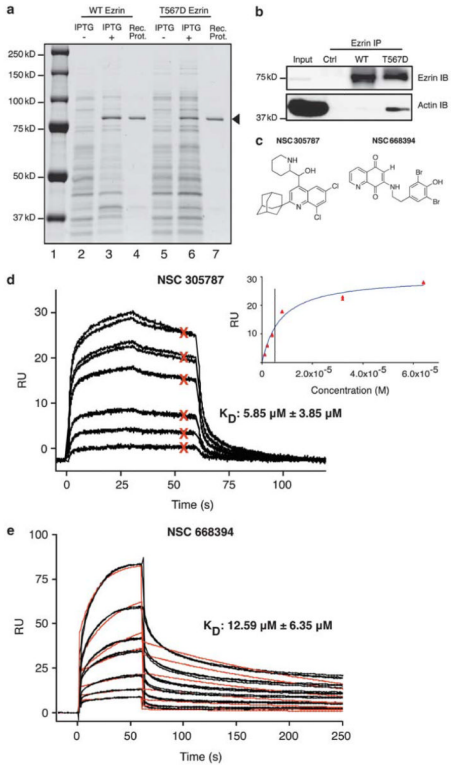

Figure 1.

NSC305787 and NSC668394 directly interact with ezrin. (**a**) WT and T567D ezrin proteins are expressed in bacteria. The most prominent band in bacterial lysates following isopropyl-beta-D-thiogalactopyranoside induction appeared just above the 75-kD molecular weight marker on a 10% polyacrylamide gel stained with coomassie blue (lanes 2 vs 3 and 5 vs 6). The best fractions from column chromatography purifications for each protein are shown in lanes 4 and 7 (arrowhead). (**b**) T567D ezrin shows stronger binding to actin than WT. K12 cell lysate was incubated with WT and T567D ezrin proteins, followed by immunoprecipitation with ezrin antibody and immunoblotting with ezrin and actin antibodies. Control (ctrl) lane is K12 lysate without recombinant protein treatment. (**c**) Chemical structures of NSC305787 and NSC668394 are given. (**d**) Direct binding of NSC305787 to WT ezrin protein was analyzed by SPR. Compound was injected at 1-, 2-, 4-, 8-, 32- and 64-μM concentrations in duplicates. A representative set of binding curves are presented with the steady-state affinity curve given in the inset. Red Xs represent binding levels that were used to calculate the steady state affinity in the inset graph. (**e**) NSC668394 was injected at 1.5-, 3-, 6-, 12.5-, 25-, 50- and 100-μM concentrations in triplicates. Black lines show actual data points, and red lines show curve fits for 1:1 binding model. Mean K_D values and standard deviations were calculated from five independent experiments for each compound.

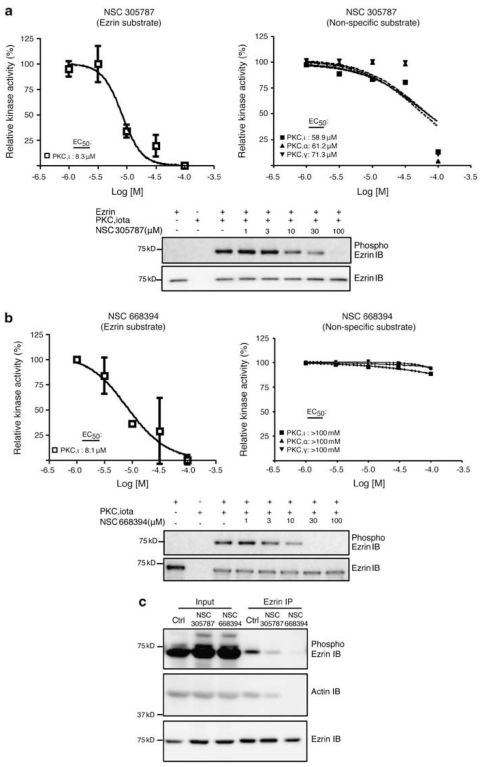

Figure 2.

NSC305787 and NSC668394 inhibit ezrin T567 phosphorylation. (**a, b**) Effect of compounds on recombinant ezrin phosphorylation by recombinant PKCI was tested in an *in vitro* kinase assay. Experiments were repeated three times, and densitometric analysis of bands was used for calculation of relative kinase activity (graphs). Error bars represent the s.d. from three independent experiments. Kinase activities of PKCI, α and γ were also evaluated with a non-specific substrate (myelin basic protein) in the presence of NSC305787 and NSC668394 using a radioactive *in vitro* kinase assay. (**c**) Both compounds inhibit phosphorylation of endogenous ezrin protein and interaction with actin without altering cellular ezrin levels. K7M2 cells were treated with NSC305787 (10 μM) and NSC668394 (10 μM) for 6 h and then subjected to immunoprecipitation with ezrin antibody followed by immunoblotting with phosphoezrin, actin and ezrin antibodies. Control (Ctrl) lane is DMSO (1%)-treated K7M2 lysate.

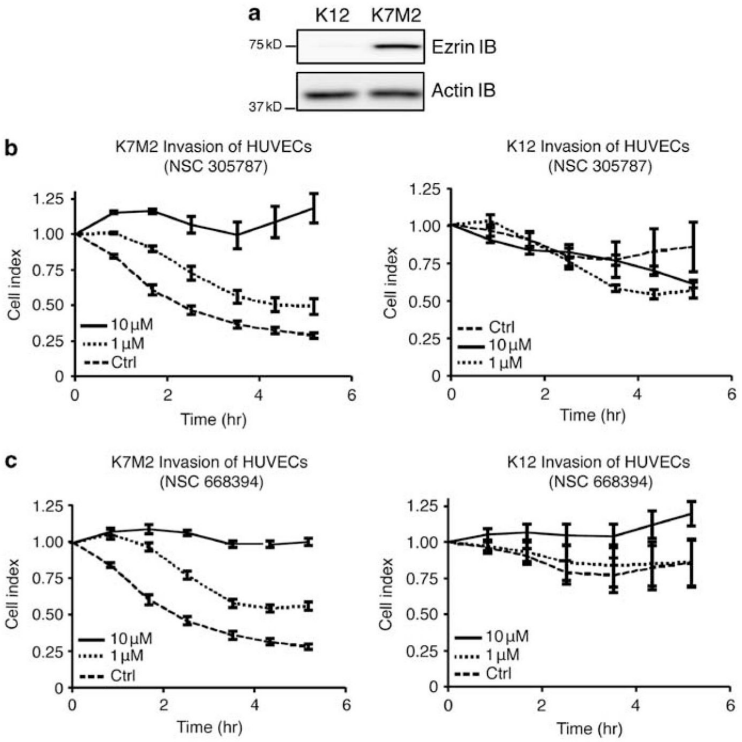

Figure 3.

NSC305787 and NSC668394 inhibit ezrin-mediated invasion of K7M2 OS cells. (**a**) Immunoblotting showed that the K7M2 cell line had higher levels of ezrin protein expression than K12 cells. (**b**, **c**) The anti-invasive potential of NSC305787 and NSC668394 was validated in K7M2 and K12 cells using an electric cell impedance system. DMSO (1%) was used as a control. Error bars represent standard deviations from duplicate data points. In this assay, a decrease in cell index represents invasion of the HUVEC monolayer by OS cells.

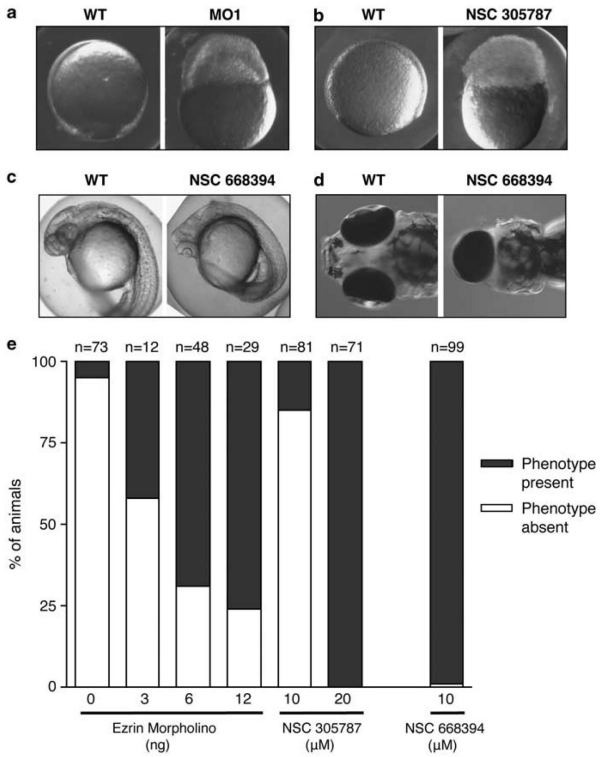

Figure 4.

NSC305787 and NSC668394 cause reduced cell motility phenotypes in zebrafish. (**a**) In the late blastula period, blastodisc cells begin to spread over the yolk cell in the process of epiboly. Reduction of ezrin protein levels by anti-sense MO results in epiboly defects characterized by cells not spreading over the yolk cell but instead piling up at the animal pole. MO-injected embryos were scored for epiboly defects at the 90% epiboly stage: WT (un-injected), 4/73 (5%); 3 ng MO, 5/12 (42%); 6 ng MO, 33/48 (69%); and 12 ng MO, 20/29 (69%). (**b**) When embryos were treated with 10-μM NSC305787, 12 of 81 embryos (15%) exhibited epiboly defects that completely mimicked MO-injected embryos. At 20-μM NSC305787, 71 of 71 embryos (100%) demonstrated epiboly defects. (**c**) Normal eye development follows lateral movement of progenitor cells to form two eyes in WT embryos. NSC668394 (10 μM) inhibited motility of eye progenitor cells, resulting in cycloptic embryos at 28 hpf in 97 of 99 embryos (98%). (**d**) NSC668394-treated embryos continued to grow and formed a single functional eye at 6 days after fertilization. (**e**) Percentages of animals with the observed phenotypes upon treatment are indicated.

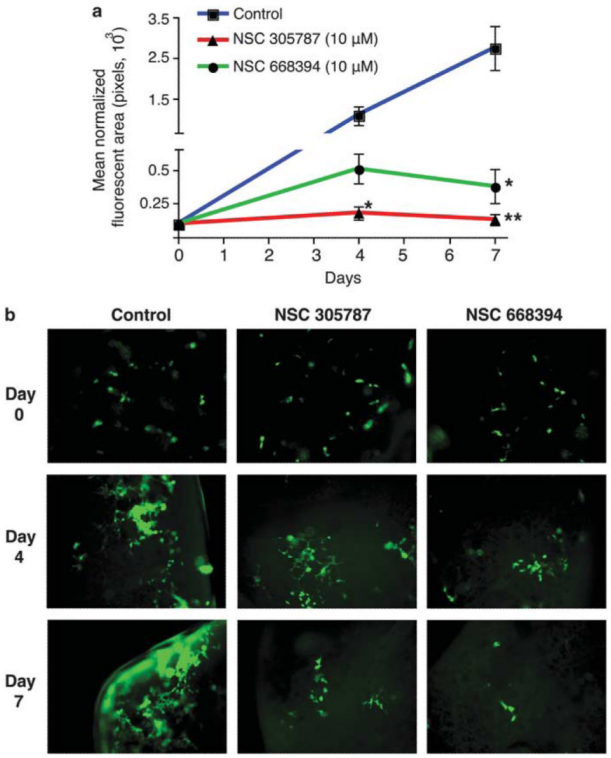

Figure 5.

NSC305787 and NSC668394 inhibit OS metastatic growth in lung organ culture. (**a**) GFP-expressing K7M2 OS cells were injected into tail veins of BALB/C mice, and the lungs were dissected. Lung slices were grown in culture media, and tumor growth was monitored. Quantitation of the fluorescence signal from NSC305787 (10 μM), NSC668394 (10 μM) and vehicle (DMSO, 1%)-treated organ cultures. Data are represented as means±s.d. from three independent experiments. (* $P<0.05$, ** $P<0.005$, using a two-tailed Student's *t*-test) (**b**) Fluorescence images of a representative culture treated with NSC305787, NSC668394 and vehicle are shown.

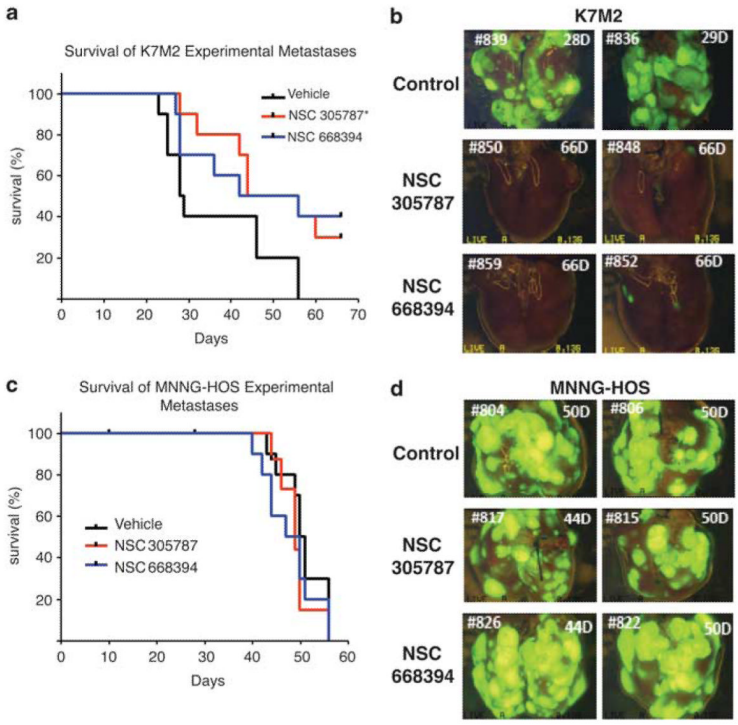

Figure 6.

NSC305787 and NSC668394 inhibit *in vivo* OS metastatic growth in lungs. (**a**) Kaplan–Meier survival curves show the percentage survival for NSC305787 and NSC668394 treatment over time in K7M2-injected animals. The overall survival of NSC305787-treated mice was significantly different than that of the vehicle-treated group and NSC668394-treated mice showed an increase in survival, but this increase was not statistically significant from the vehicle group (*P*-value of NSC305787 is 0.0337 and NSC668394 is 0.0524). Log-rank statistics were used for survival curves. (**b**) Representative fluorescence images of whole lungs at the time of necropsy are shown. (**c**) Survival ratios of the groups were not different because MNNG-HOS is an ezrin-independent cell line. (**d**) Representative fluorescence images of whole lungs from MNNG-HOS-injected animals at the time of necropsy are shown.